The Solar Atmosphere

Article *in* Lecture Notes in Physics · April 2009

DOI: 10.1007/978-3-642-00210-6_4

CITATIONS
2

READS
1,080

2 authors:

Viggo H. Hansteen
University of Oslo
213 PUBLICATIONS **6,802** CITATIONS
SEE PROFILE

Mats Carlsson
University of Oslo
310 PUBLICATIONS **8,825** CITATIONS
SEE PROFILE

The Solar Atmosphere

Viggo H. Hansteen and Mats Carlsson

Institute of Theoretical Astrophysics, University of Oslo
PB 1029 Blindern, 0315 Oslo, Norway
viggo.hansteen@astro.uio.no

1 Introduction

Looking at the solar photosphere, we see the top of the convection zone in the form of granulation: Hot gas rising from the solar interior as part of the energy transport process reaches a position where the opacity is no longer sufficient to prevent the escape of radiation. The gas expands, radiates, and cools and in so doing loses its buoyancy and descends. These motions, ultimately driven by the requirement that the energy generated by nuclear fusion in the Sun's core be transported in the most efficient manner, represent a vast reservoir of "mechanical" energy flux.

Looking closer, we see that granulation is not the only phenomenon visible at the solar surface. The quiet and semi-quiet photosphere is also threaded by magnetic fields that appear as bright points, as well as darker micro-pores and pores. These small scale magnetic structures are, while able to modify photospheric emission, subject to granular flows and seem to be passively carried by the convective motions.

Convective flows are also known to generate the perturbations that drive solar oscillations. Oscillations, sound waves, with frequencies mainly in the band centered roughly at 3 mHz or 5 minutes are omnipresent in the solar photosphere and are collectively known as p-modes ('p' for pressure). These p-modes are a subject in their own right and studies of their properties have given solar physicists a unique tool in gathering information on solar structure — the variation of the speed of sound c_s, the rotation rate, and other important quantities — at depths far below those accessible through direct observations. In this chapter we will consider them only insofar as they interact and possibly channel energy into the layers above the photosphere.

The shuffling, buffeting, and braiding of magnetic structures that presumably continue on up into the upper solar layers, the propagation of the higher frequency component [1] photospheric oscillations through the chromosphere and into the corona — all may contribute to heating and thus the production

[1] Waves with frequencies lower than the acoustic cutoff frequency of roughly 5 mHz are evanescent above the photosphere and do not propagate energy into the higher solar atmosphere (unless the magnetic field topology can modify the frequency at which waves become evanescent).

of a 1 MK or hotter corona. But in what proportion? And by how much? And what are the observational signatures of the various possible heating sources?

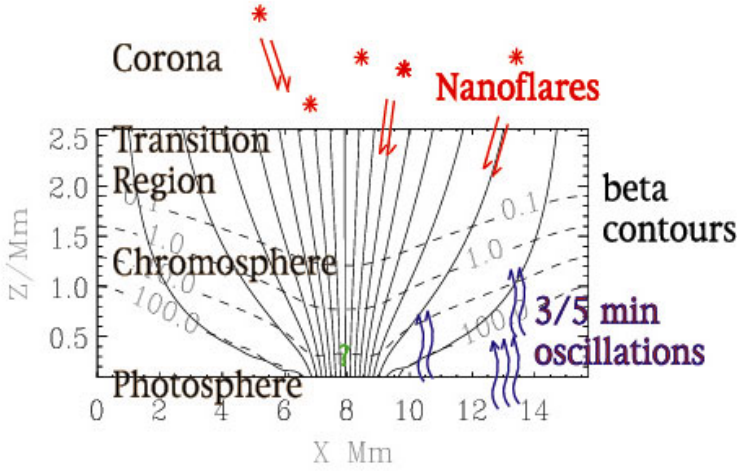

Fig. 1. Schematic view of the structure of the solar atmosphere: In the photosphere the gas pressure is larger than the magnetic pressure and photospheric motions are driven by convection — a mainly hydrodynamic phenomenon that brings up new magnetic flux, buffets and reorganizes existing field. Oscillations of somewhat higher frequency than the photospherically dominant 5 minute oscillations propagate into the chromosphere. Upon reaching the level where the exponentially decreasing gas pressure becomes equal to the magnetic pressure, the surviving sound waves may be converted into other wave modes. It is likely that the processes heating the corona and magnetic chromosphere are episodic; this will likely induce large temperature differences, flows and other non-steady phenomena that will produce other wave modes, perhaps with observable signatures.

The structure and the topics of this chapter are summarized in figure 1. We will consider a photosphere in continual motion, threaded by magnetic fields and subject to 5-minute oscillations. Currently, *e.g* with the Swedish Solar Telescope on La Palma, and in the near future, with the JAXA's Solar-B satellite, we will have access to visible wavelength observations of the photosphere and its attendant fields with a spatial resolution of roughly 0.1 – 0.2 arsec, equivalent to 75 – 150 km on the solar surface. Careful analysis of this wealth of observational data on the "lower boundary" of the corona should eventually yield insight into the mechanism(s) heating the corona and chromosphere.

On average the photospheric gas pressure is $p_g = 10^4$ N/m^2 which is much greater than the pressure represented by an average unsigned magnetic field

strength of 1 – 10 Gauss that is observed. However, in the largely isothermal chromosphere the gas pressure falls exponentially, with a scale height of some 200 km, while the magnetic field strength falls off much less rapidly, even as the field expands and fills all space. Thus, and depending on the actual magnetic field topology, the magnetic pressure and energy density will surpass the gas pressure some 1500 km or so above the photosphere in the mid chromosphere. Another 1000 km, or 5 scale heights above the level where $\beta = 1$ (β is defined as the ratio of the gas pressure and the magnetic pressure), the plasma's ability to radiate becomes progressively worse, while the dominance of the magnetic field becomes steadily greater. Any given heat input cannot be radiated away and will invariably raise the gas temperature to 1 MK or greater; a corona is formed. A corona that is bound to follow the evolution of magnetic field as the field in turn is bound to photospheric driving.

2 The Photosphere

Solar convective motions continuously churn the outer solar atmosphere. Hot, high entropy gas is brought up to the photosphere where the excess energy is radiated away. Cool low entropy material descends into the depths in steadily narrower lanes and plumes as explained in the numerical models of Stein & Nordlund [1]. The result of these motions is, of course, the granular pattern observed on the solar surface and described in countless papers and textbooks.

Recounting this wealth of knowledge falls far outside the scope of this chapter. We will rather describe a limited set of recent observations made at the Swedish Solar Telescope with special attention paid to observations of the structure and dynamics of photospheric bright points. These observations are indicative of the quality of data that will arrive with the launch of the Japanese Solar B satellite from which we can expect images and spectra, including vector magnetograms and dopplergrams from the photosphere with a spatial resolution of roughly 0.2 arcsec.

2.1 Recent observations

In figures 2 and 3 we show typical images of the quiet to semi-quiet photosphere as well as a plage region. These images are made in the so called G-band centered around 430 nm which is formed some 100 km above the nominal photosphere. The observations were obtained with the Swedish 1-meter Solar Telescope [2] on La Palma. Details of the optical setup and instrumentation are described in [3].

Narrow-band interference filters were used for quasi-simultaneous imaging in the line core of the Ca II H line (396.9 nm, filter passband 0.3 nm), the G-band (430.5 nm) and near-by continuum (436.4 nm, G-cont).

In the work described here seeing effects were reduced using several complementary techniques: Adaptive optics [4] utilizing both a tip-tilt mirror and a deformable mirror, real-time frame selection, and post-processing using the Multi Object Multi Frame Blind Deconvolution (MOMFBD) image reconstruction technique [5]. The latter allows one to build up long time series of very high quality data, vital to the imaging of time dependent phenomena on the solar surface.

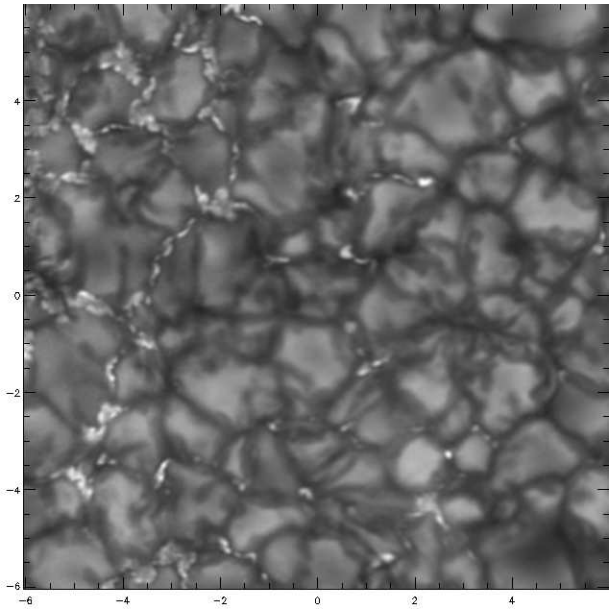

Fig. 2. A typical quiet photospheric region observed in the G-band with the Swedish Solar Telescope. This spectral band formed near 430 nm contains several spectral lines (see figure 4) and notably the lines of the CH-molecule, is formed near the height where $\tau_{500\ nm} = 1$; granulation and intergranular lanes some 100 km above this height, bright points some 200 km below — as explained in the text in connection with figure 5. Bright points are regions of enhanced magnetic field concentrated and contained by the granular motions. Notice also that bright points are pulled into ribbons and fill the entire intergranular lane.

In figure 2 we show examples of simple bright points in a fairly quiet region of the photosphere. Isolated bright points are constrained to intergranular lanes and do not seem to have any internal structure. Isolated bright points appear to be passively advected towards the periphery of supergranular cells [6], where they gather and form the magnetic network.

Several studies of the statistical properties of the dynamical evolution of bright points have appeared in the literature. Berger & Title (1996) [7] described a number of effects during the lifetime of bright points. These

include shape modifications such as elongation, rotation, folding, splitting and merging. Significant morphological changes can occur on time scales as short as 100 s and are strongly dependent on the local granular convective flow field. These changes make it difficult to define a typical lifetime of bright points. Berger et al. (1998) [8] found an average lifetime of 9.3 min using automated feature tracking techniques on a 70 min sequence of enhanced magnetic network. Some bright points persist up to the entire 70 min, and they experience numerous merging and splitting events but are still regarded as single objects. In a study of isolated bright points in a network region, Nisenson et al. (2003) [9] found a similar mean lifetime of 9.2 min with the longest-lived bright point lasting 25 min. These reported values for the mean lifetime are very similar to the evolution time scale of granulation.

Towards the left side of figure 2 we see examples of bright points forming ribbon-like shapes in the intergranular lanes. In places these ribbons surround entire granules. Circular manifestations of these spread out, ribbon-like structures, are dubbed "flowers", of which many examples are found in figure 3. This figure shows a region of stronger average field strength than does figure 2. The "flowers" and diverging ribbons have typical scales smaller than 1 arcsec. Flux concentrations with larger spatial extent are embedded in (micro-)pores with distinctly dark centers. In these more active areas there is a much greater density of bright points. They take on structure and appear to modify the granular flow itself. Granules near network bright points and in plage regions are smaller, have lower contrast and display slower temporal behavior. The granular pattern in these magnetically dominated areas are referred to as "abnormal". Coalescing bright points in plage and network regions form dark centers and thus become micropores.

In order for these magnetic structures to become visible at all they must attain field strengths of sufficient amplitude to perturb the plasma they are embedded in, (even while being passively advected). Thus, we expect that there also exists a whole hierarchy of magnetic structures which have not yet attained such a critical field strength. What is the source of this field? One possible scenario is that it is brought up in granules at field strengths too low to leave an observational signature in the photospheric intensity. Granular flow then carries the field to the intergranular lanes and ultimately to the intergranular intersections where it may become compressed and strong enough to make the field visible, i.e. on the order of 1500 Gauss for a photospheric pressure of 10^4 N/m^2. This then would be the reason bright points always seem to appear in intergranular intersections.

2.2 Why bright points?

Photospheric bright points are correlated with regions of strong magnetic field and are subject to photospheric motions. Plage regions share similar characteristics but seem capable of modifying the background flow. Enhanced emission implies high temperatures, on the other hand, micropores, pores,

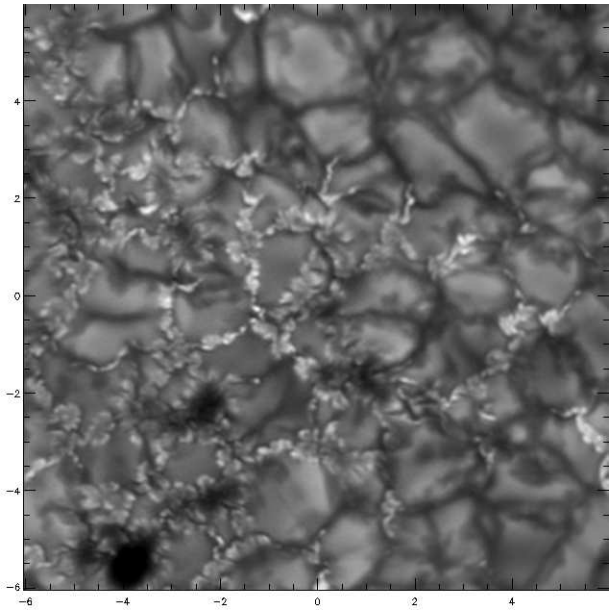

Fig. 3. A photospheric plage region observed with the Swedish Solar Telescope in the G-band. Notice the large number of phenomena showing complex structure; ribbons, flowers, micropores, as well as isolated and seemingly simple bright points. The magnetic field is in this image in places strong enough to perturb granulation dynamics and the granules appear "abnormal" while displaying a slower evolution than in the quieter photosphere.

and sunspots are dark. What is the relation between magnetic fields and the photospheric and lower chromospheric temperatures? Why are bright points bright?

One way to answer this question is through atmospheric modeling of the relevant phenomena using the MHD equations given by

$$
\begin{aligned}
\frac{\partial \rho}{\partial t} + \nabla \cdot \big(\rho \mathbf{u}\big) &= 0 \ , \\
\frac{\partial e}{\partial t} + \nabla (e\mathbf{u}) + \mathbf{u} \cdot \nabla p_g &= \nabla \mathbf{F}_{\rm r} + \nabla \mathbf{F}_{\rm c} + Q_{\rm Joule}, \\
\frac{\partial \mathbf{B}}{\partial t} - \nabla \times \big(\mathbf{u} \times \mathbf{B}\big) &= 0 \ , \\
\frac{\partial \mathbf{u}}{\partial t} + \big(\mathbf{u} \cdot \nabla\big)\mathbf{u} + \frac{1}{\rho}\nabla p &= \frac{1}{4\pi\rho}\big(\nabla \times \mathbf{B}\big) \times \mathbf{B} - g\hat{\mathbf{z}} \ , \\
e \ &= \ \frac{1}{\gamma - 1}\frac{p}{\rho} \ ,
\end{aligned}
$$

where $\mathbf{F}_{\rm r}$ represents the radiative flux, $\mathbf{F}_{\rm c}$ represents the conductive flux, $Q_{\rm Joule}$ is the joule heating and all other symbols have their usual interpretation.

Photospheric convection is driven by the radiative losses from the solar surface. In order to model granulation correctly it is vital to construct a proper model of of radiative transport. A sophisticated treatment of this difficult problem was devised by Nordlund in 1982 [10] in which opacities are binned according to their magnitude; in effect one is constructing wavelength bins that represent stronger and weaker lines and the continuum so that radiation in all atmospheric regions is treated to a certain approximation. In general, the radiative flux divergence from the photosphere and lower chromosphere is obtained by angle and wavelength integration of the the transport equation. Also, assuming isotropic opacity and emissivity one finds

$$\nabla \mathbf{F}_{\rm r} = 4\pi \int_{\lambda} \epsilon_{\lambda} \chi_{\lambda} (B_{\lambda} - J_{\lambda}) d\lambda \tag{1}$$

If one further assumes that opacities are in LTE the radiation from the photosphere can be modeled[2]. After binning the opacities at all wavelengths in groups the group mean opacities are used in calculating a group mean source function from which the emergent intensity, and thus the radiative losses, can be derived by standard methods such as Feautriers formal solver.

This method of approximating solar radiative transport coupled with a MHD numerical code allows one to model solar convection with a high degree of realism [10]. Carlsson *et al.* [12] constructed convection simulations such as these in which, in addition, an initial vertical magnetic field of magnitude 250 Gauss was inserted. The equations were discretized on a numerical grid of $253\times253\times163$ points covering $6\times6\times2$ Mm^3. With time the magnetic field was carried along with the convective flow and formed quite complex topologies.

Once the model has evolved to a quasi steady state synthetic spectra of the G-band (or any other wavelength band formed in the modeled region) can be computed *a posteriori* using a radiative transfer code containing more than the essentially four frequency points used in the MHD simulation. In the results presented here this was done using a spectral model with 2728 frequency points representing emission from 845 lines for the G-band as shown in figure 4. Note the excellent agreement between the average synthetic spectrum shown in black and an average photospheric spectrum shown in red. The model contains essentially no free parameters (other than the initial magnetic field strength which value does not change the average computed spectrum to any noticeable degree). This agreement is fairly strong evidence that most of the relevant physics is included in the model.

[2] The effects of coherent scattering may be incorporated if one wants to model the lower and mid chromosphere. The resulting 3d scattering problems are then solved by iteration based on a one-ray approximation in the angle integral for the mean intensity, a method developed by Skartlien 2000 [11]

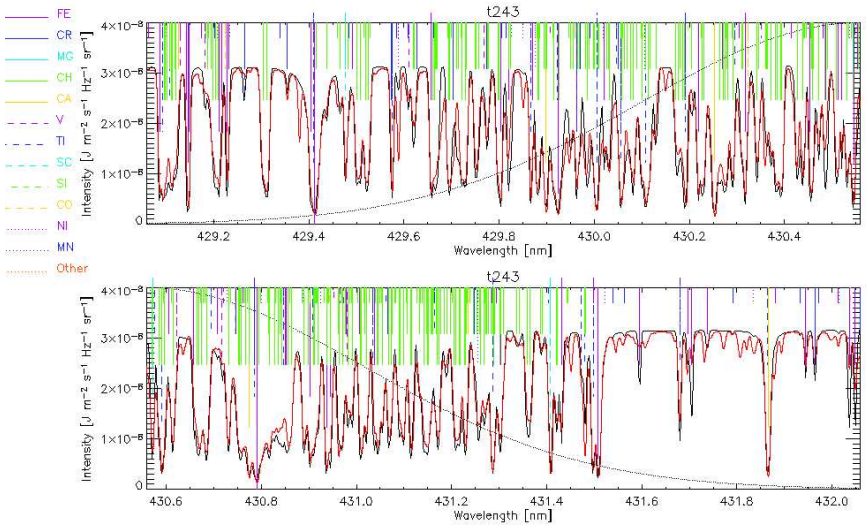

Fig. 4. The solar spectrum in the region of the G-band located near 430 nm. The bandpass of the filter used in obtaining figures 2 and 3 is shown by the dotted line. A great number of lines constitute this spectral band, lines from the CH molecule are prevalent, but also many other elements are represented. The observed spectrum of the solar photosphere is shown by the red line, the modeled spectrum is shown in black; for details of the model see the text or Carlsson et al. [12].

The advantage of having a model of the phenomena is clear: One can look at any given variable as a function of position and time. Armed with these results one is in a position to describe the emission from various photospheric regions; from a granule, from an intergranular lane, from a bright point, and from the region of strongest magnetic field concentration in the model.

The increased brightness in magnetic elements is due to their lower density compared with the surrounding intergranular medium. One thus sees deeper layers where the temperature is higher. At a given geometric height, the magnetic elements are cooler than the surrounding medium because the magnetic fields prevent convective energy transport from deeper layers. At the edges of the flux concentrations the plasma is radiatively heated by the surrounding hotter, non-magnetic plasma. See figure 5 for examples of the temperature structure and heights of emergent intensity formation for four different positions in the model.

3 The Chromosphere

With the observations and modeling of photospheric granulation and bright points discussed in section 2.1 in mind let us turn to the chromosphere. What

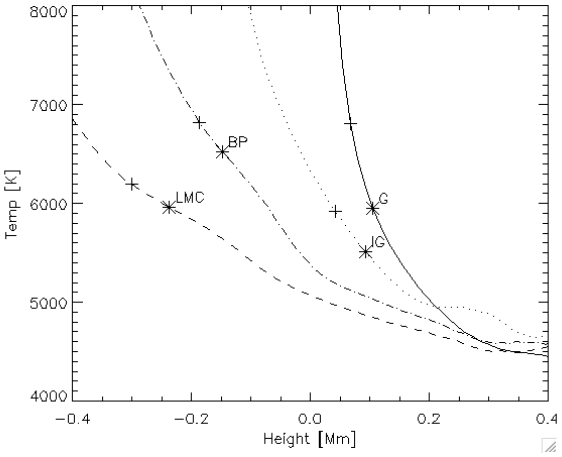

Fig. 5. The gas temperature as a function of height for four positions in the model of Carlsson et al. [12]: The curves marked 'G' and 'IG' represent positions in a typical granule center and intergranular lane. The asterisk show the formation height where the G-band is formed; emergent radiation from the granule center is formed at a higher temperature and thus appears brighter than the intergranular lane. The curves marked 'BP' and 'LMC' represent a bright point and the region of greatest magnetic field concentration; the bright point appears bright as the opacity is low enough to sample gas as great depths, even though at any geometric point in the simulation the temperature is higher in both granules and intergranular lanes. The same is also true for the region of greatest magnetic field, strong enough to hinder convection and large enough horizontally to hinder radiative heating from the 'walls' of the flux tube.

happens as perturbations implied in photospheric granulation propagate upward? How does the magnetic field expand into the overlying regions? and how does this change the dynamics of the atmosphere the field is expanding into?

Originally the chromosphere — *i.e. colored sphere* — has its name from eclipse observations. One can occasionally observe the strong intensely red light stemming from the H-α line circumscribing the solar limb. The chromosphere is much thicker than the photosphere; it contains roughly $10 - 12$ scale heights of say 200 km each and hence stretches some 2500 km between the photosphere and transition region.

3.1 Chromospheric Oscillations

Much work has gone into the elucidation of the thermal structure of the chromosphere and the mechanical heating needed in order to maintain this structure against radiative losses. Seminal in this regard is the work of Gene Avrett and co-workers in the 1980's [13]. However, we would like to approach chromospheric structure from another angle.

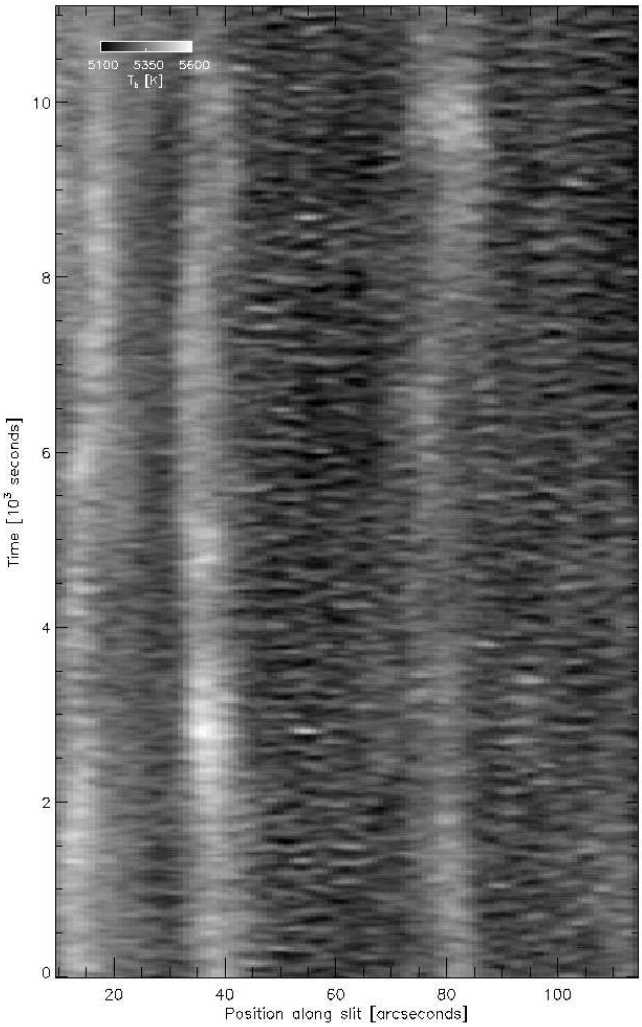

Fig. 6. Chromospheric oscillations as seen in the C continuum formed near 104 nm at a height roughly 1100 km above the photosphere. This observation is made by pointing the SUMER slit at a given, quiet sun, location of the sun and making an exposure every 20 s or so. The image is made by stacking consecutive exposures of the slit vertically to form an image. The brighter vertical bands represent areas of enhanced magnetic field. The horizontal structures most clearly visible between the bright vertical bands can be explained by upwardly propagating 5 mHz oscillations. See Wikstøl et al. [14].

Assume that the chromosphere be considered an initially isothermal slab stratified by a constant gravitational acceleration g. Then the linearized equations of mass, momentum and energy conservation [15]

$$\frac{\partial}{\partial t}\delta\rho + \rho_0\frac{\partial}{\partial z}\delta u + \delta u\frac{\partial \rho_0}{\partial z} = 0,$$

$$\rho_0\frac{\partial}{\partial t}\delta u = -\frac{\partial}{\partial z}\delta p - g\delta\rho,$$

and

$$\frac{\partial}{\partial z}(\delta p - c_s^2\delta\rho) + \rho_0^\gamma \delta u\frac{\partial}{\partial z}\left(\frac{p_0}{\rho_0^\gamma}\right) = 0.$$

The subscript "0" denotes unperturbed quantities, the vertical velocity is denoted u, while $c_s = \sqrt{\gamma p_0/\rho_0}$ and p are the speed of sound and the gas pressure, respectively.

These equations may be combined into

$$\frac{\partial^2 Q}{\partial t^2} - c_s^2\frac{\partial^2 Q}{\partial z^2} + \omega_a Q = 0 \tag{2}$$

where $Q \equiv \rho_0(z)^{1/2}u$ and the acoustic cutoff frequency is $\omega_a \equiv c_s/2H_p = \gamma g/2c_s$. This is a Klein-Gordon equation, the solution of which, after eventual initial transients have died down, is an oscillatory wake with a period close to the acoustic cut-off frequency. If we imagine photospheric dynamics as a driver — a driver with typical driving frequencies in the 5 minute/3 mHz band, along with other excitations due to individual granule dynamics — we therefore expect on the basis of equation 2 the chromospheric response to be an oscillation with a frequency near 5 mHz corresponding to a period of roughly 3 minutes. Note that this conclusion is taken without any consideration of effects such as radiative damping or close consideration of the driver spectrum.

Be that as it may, in many cases a chromosphere dominated by 3 min power is indeed what is found. In figure 6 we see continuum emission in the 104.3 nm band observed with the SUMER instrument aboard the SOHO satellite. The image is made by stacking consecutive exposures of the slit vertically as a function of time. Note the horizontal bands of enhanced emission with horizontal extent on the order of tens of arcseconds that recur with a period of roughly 3 minutes. These horizontal bands are omnipresent in the image presented here and can be explained as a result of upwardly propagating wave-trains.

In fact, Carlsson & Stein [16] have shown that many aspects of the internetwork chromosphere can be explained as a result of photospheric excited, upwardly propagating acoustic waves. In their simulations a photospheric driver, a piston taken from the doppler velocities measured in a Fe I line, formed in the photosphere, is used to excite waves. These waves propagate upward, and as they do so their amplitude grows, steepens and forms shocks.

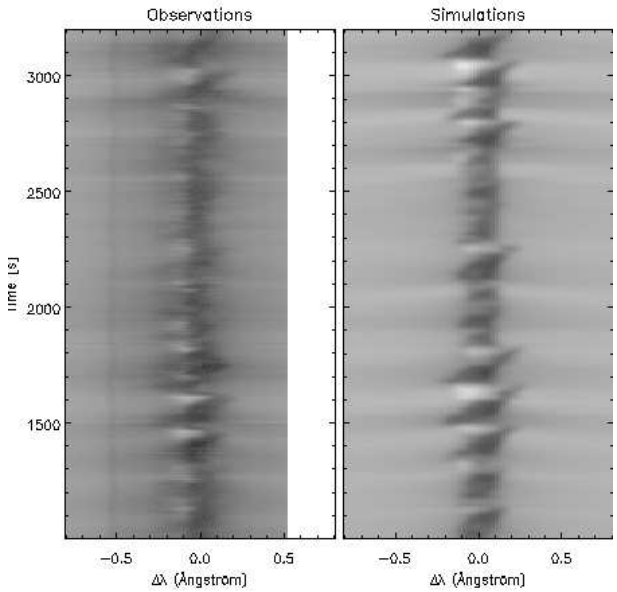

Fig. 7. The Ca II H-line profile as a function of time. Multiple repeated exposures are made with a slit fixed at a given position on the sun. The observed line profile in a quiet, internetwork, position is shown in the left panel. A 1d radiation-hydrodynamic model due Carlsson & Stein 1995 [16], containing upwardly propagating acoustic waves driven by a piston computed from the doppler shift measured in an Fe I line in the blue wing results in the Ca II H-line profiles shown in the right panel. Waves appear in the line wings and propagate towards line center as the acoustic wave moves upward in the atmosphere. A peak brightening on the violet side of the line core, formed some 1000 km above the photosphere, indicates that the wave amplitude has grown and that the wave is non-linear.

A self-consistent radiative transfer calculation produces energy transfer in the model as well as diagnostics, especially in the Ca II H line. The results of the model are shown in figure 7 which displays the observed and computed Ca II spectra as a function of wavelength and time. The figure shows the general behavior of the line emission in both observation and simulation: Enhanced emission arises first in the line wings and thereafter moves in towards the line core. This emission is consistent with an upwardly propagating wave; emission formed far out in the line wings is formed at lower heights than that formed near the core. Upon reaching the core the perturbation causes the blue, or violet, peak to become very enhanced while a corresponding red peak is mostly absent. This anisotropy is a signature of a large velocity gradient in the region of emission formation, *i.e.* the wave has formed a shock at the height where the K2V peak is formed, roughly 1000 km above the photosphere (where $\tau_{500\ nm} = 1$). It is also worth noticing that even the details

of Ca II emission are reproduced in this model. Comparing individual peaks show that they are similar in both timing and intensity in observation and model.

These and similar simulations also show that the results indicated by the linear analysis is essentially correct: waves with frequencies lower than the acoustic cutoff frequency at roughly 5 mHz decay exponentially with height in the chromosphere. As shown above, waves are naturally excited at the cut-off frequency of 5 mHz as wake oscillations. However, the simulations mentioned above show that the most important reason for a powerpeak at 5 mHz in the chromosphere is the exponential damping of the lower frequency, non-propagating waves. A photospheric spectrum dominated by 3 mHz waves with wave-power decreasing with frequency above 3 mHz will change in height to become dominated by the lowest propagating, non-damped, frequencies. Waves with frequencies much above 5 mHz could in principle propagate up into the upper chromosphere and play an important role. However, high frequency waves are a) not strongly excited by photospheric motions and b) are very strongly radiatively damped as they propagate, the damping increasing with increasing frequency [17]. Thus only waves with frequencies in the range 5 to, say, 10 mHz already present in the photosphere propagate up and dominate internetwork chromospheric dynamics as they steepen and form shocks in the mid chromosphere.

There is therefore very strong evidence that the internetwork chromosphere is very dynamic and that the variations in physical quantities such as the temperature may be as large as the quantities themselves. In addition, these models show the grave danger posed by forming time average models based on diagnostics that have a non-linear response to variations in the atmosphere. There is for example no need for a chromospheric temperature rise in order to explain the behavior of the Ca II line emission in the internetwork.

3.2 The Chromospheric Network

There are however, several mysteries remaining in explaining chromospheric emission. Let us return to the upper chromosphere as imaged in figure 6. Not mentioned so far are the bright 10 arsecond or so wide vertical bands. These regions coincide with regions of enhanced photospheric magnetic field. In addition, even the background emission in the dark internetwork bands is greater than that which can be explained solely by acoustic waves. Clearly, additional heating is required, a heating which presumably is connected in some way to the magnetic field.

As magnetic bright points are advected with the granular flow they tend to concentrate in a granular pattern with typical horizontal dimensions of 20 arcseconds that defines the supergranular flow field. The chromospheric network is the manifestation of this flow field as seen in lines and continua formed in the chromosphere. In figure 8 we see the chromospheric network clearly outlined at greater scales than that of the the granular network seen

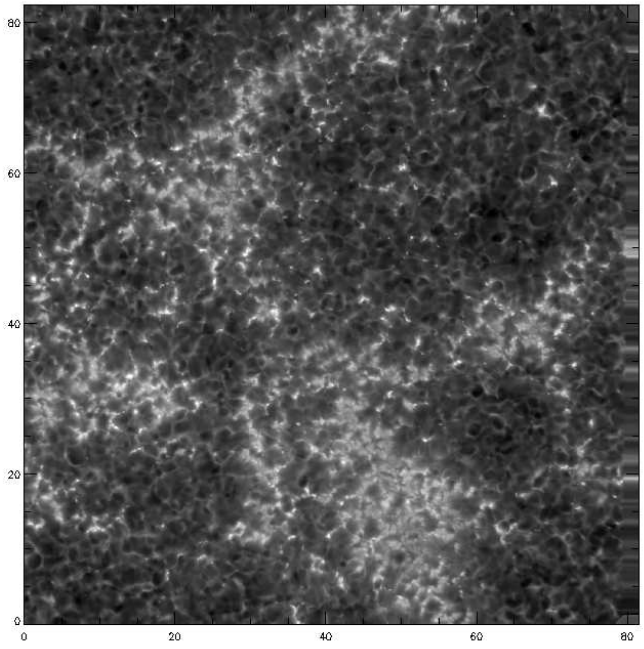

Fig. 8. The chromospheric network as observed with the Swedish Solar Telescope in the Ca II H-line band. Most emission in this image is formed some hundreds of kilometers above the photosphere. We see inverse granulation, an image of the 'overshoot' of vertical granular flow with horizontal scales identical to that of regular granulation. Magnetic bright points are advected with the granular flow and are transported to the chromospheric network which forms a granular pattern with horizontal size scales of 20 arcseconds or so.

in the form of inverse granulation in this image. The inverse granulation is a hydrodynamic phenomena caused by the previously hotter granules rising, expanding and cooling, whereupon the gas is compressed it begins to fall back towards the lower photosphere and converges with the flow from other expended granules. The network emission, on the other hand, seems to be caused by an enhanced heating due to the magnetic field, the nature of which is still unknown.

The magnitude of the magnetic field in the chromosphere (and corona) can be estimated by potential field extrapolations from the measured longitudinal field in the photosphere. This is done by solving the equation

$$\nabla \times \mathbf{B} = 0$$

with the boundary condition $B_z(x, y, 0) = B_{z0}(x, y)$ using an appropriate method [18]. Alternately one can carry out force free calculations with a constant α, or non-linear force free calculations by various methods as surveyed

by Schrijver *et al.* [19]. Extrapolations show that magnetic field will penetrate to a height that is roughly equal to the separation between sources. Thus, granular scale field will reach heights equivalent to a few arcseconds; *i.e.* 1000 km or so, while fields on network scales will reach high into the corona, on the order 20 – 30 Mm. Typical photospheric field strengths, which could vary from some few Gauss to 1000 Gauss or more, will dominate the gas pressure at heights varying from some few scale heights above the photosphere to a height of 1500 km or more. In other words, we can expect the surface where $\beta = 1$ to be very corrugated.

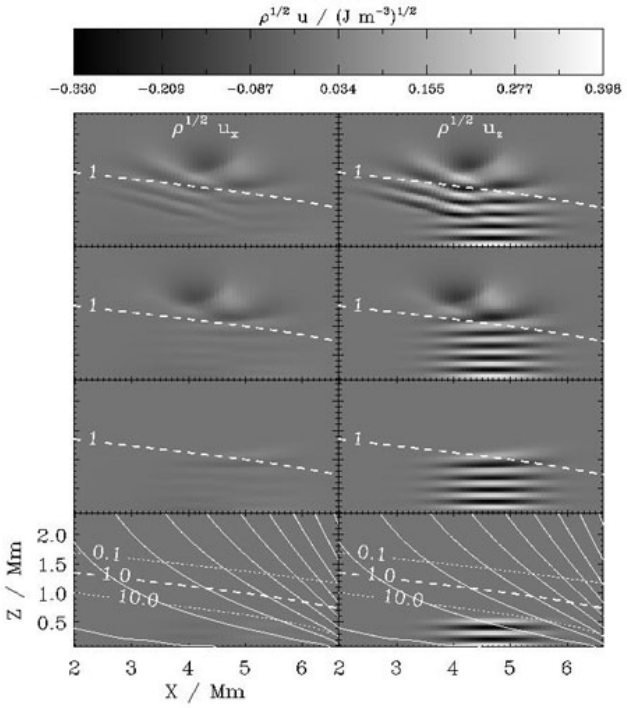

Fig. 9. Plots of the horizontal (left panels) and vertical velocities scaled with the square root of the density. In this model a schematic isothermal chromosphere with magnetic field structure shown by the solid lines and the position of plasma β by the dashed lines in the lower panels. A fast mode (acoustic) wave is excited at the lower boundary by a vertically moving piston. The fast mode wave interacts with the magnetic field near $\beta = 1$ such that the wave is refracted and essentially reflected back into the photosphere and towards regions of high plasma β. See Rosenthal et al. 2002, Bodgan et al. 2003 [20, 21].

We have seen that we expect a multitude of waves and wave modes to be excited in the solar convection zone. In most of the convection zone, the excited waves will be predominantly acoustic in nature. When acoustic waves reach the height where the Alfvén speed is comparable to the sound speed, *i.e* roughly where $\beta = 1$, they undergo mode conversion, refraction and reflection. In an inhomogeneous, dynamic chromosphere this region of mode conversion will be very irregular and change in time. We thus expect complex patterns of wave interactions that are highly variable in time and space.

What happens to these acoustic waves as they propagate from the photosphere into the chromosphere? McIntosh and co-workers have found that there is a clear correlation between observations of wavepower in SOHO/SUMER observations and the magnetic field topology as found from potential field extrapolations based on from SOHO/MDI observations of the longitudinal magnetic field [22, 23].

An understanding of the basic phenomena can be built up by studying some simplified cases. Rosenthal and co-workers [20] made 2D simulations of the propagation of waves through a number of simple field geometries in order to obtain a better insight into the effect of differing field structures on the wave speeds, amplitudes, polarization, direction of propagation etc. In particular, they studied oscillations in the chromospheric network and internetwork. They find that acoustic, fast mode waves in the photosphere become mostly transverse, magnetic fast mode waves when crossing a magnetic canopy where the field is significantly inclined to the vertical, as shown in figure 9. Refraction by the rapidly increasing phase speed of the fast mode waves results in total internal reflection of the waves.

This work was extended to other field geometries, resembling a sunspot [21]. Four cases are studied; excitation by either a radial or a transverse sinusoidal perturbation and two magnetic field strengths - either an "umbra" at the bottom boundary or a weak-field case. In the strong field case the plasma β is below unity at the location of the piston and the upward propagating waves do not cross a magnetic canopy. As the field is not exactly vertical at the location of the piston, both longitudinal and transverse waves are excited. The longitudinal waves propagate as slow mode, predominantly acoustic, waves along the magnetic field. The transverse waves propagate as fast mode, predominantly magnetic, waves. These waves are not confined by the magnetic field and they are refracted towards regions of lower Alfvén speed. They are therefore turned around and they impinge on the magnetic canopy in the "penumbral" region. In places where the wave vector forms a small angle to the field-lines, the waves are converted to slow waves in the lower region; in places where the attack angle is large there is no mode conversion and the waves continue across the canopy as fast waves. The simulations show that wave mixing and interference are important aspects of oscillatory phenomena.

4 Coronal Heating

The problem of coronal heating has plagued solar physics since the discovery in the 1930's by Edlén and Grotrian that the corona had a temperature of order 1 MK. To this we can also add the problem of heating the network chromosphere, as well as the background emission in the internetwork chromosphere, neither of which can be explained by the action of 3 mHz or higher frequency acoustic waves.

Clearly some "mechanical" form of heat input is necessary to raise the coronal plasma to a temperature much higher than the photospheric radiation temperature. The debate has raged in the decades that have followed: The convection zone produces more than enough mechanical energy flux, but how is this energy flux transported to the corona, and how is it ultimately dissipated? Should one consider the buffeting of magnetic flux tubes on relatively short timescales, causing wave- or so called AC-heating. Or is it more appropriate to see the slower shuffling of flux tubes, causing stresses in the coronal magnetic field to build up, later to be episodically relieved in nano-flares as in the DC-heating scenario.

Even having answered that question, several remain. How is the energy flux ultimately thermalized? Do we need to continually inject new magnetic flux into the photosphere in order to sustain the corona? And if so, how much? Are there robust diagnostics that can separate the various heating mechanisms?

For reasons of personal preference we will unashamedly pursue the nano-flare heating mechanism for the duration of this chapter, but please keep in mind that this is a problem not solved. By any means!

Why MK?

Before turning to a discussion of coronal modeling and coronal heating it is worth spending a paragraph or so on coronal temperatures. Why is the coronal temperature of order 1 MK? Is achieving such a temperature a robust measure of heating mechanism success? To answer that question it is important to realize that the temperature of a plasma is set not only by the heat dissipated but also by the plasma's ability to lose energy.

The coronal plasma has essentially three possible ways to shed energy:

1. Through optically thin radiation given by
$$n_{\mathrm{e}} n_{\mathrm{H}} f(T_{\mathrm{e}})$$
where n_{e} and n_{H} are the electron and total hydrogen densities and $f(T_{\mathrm{e}}$ is a function of temperature dependent mainly on line emission and, at higher temperatures, on thermal bremssträlung.
2. Through thermal conduction along the magnetic field, with a conduction coefficient
$$-\kappa_0 T_{\mathrm{e}}^{5/2} \nabla_{\parallel} T_{\mathrm{e}}$$

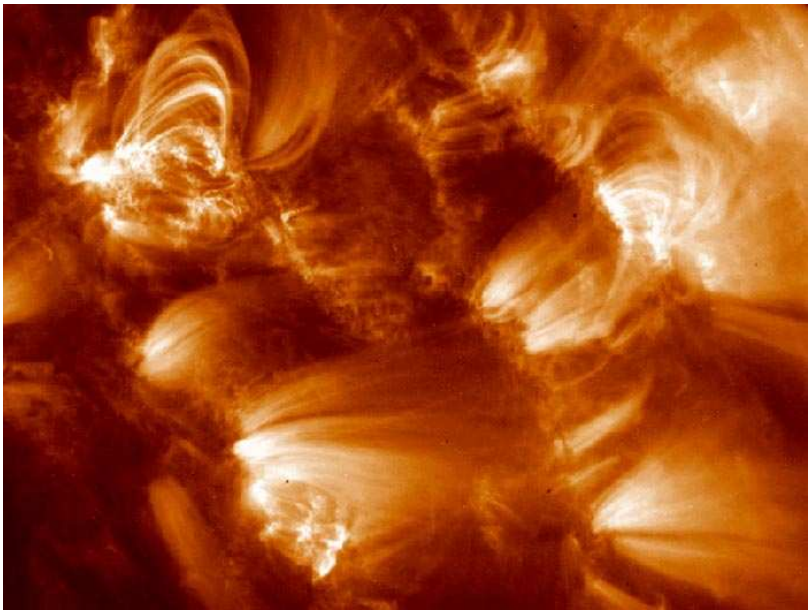

Fig. 10. The corona as seen by the TRACE telescope (TRACE, is a mission of the Stanford-Lockheed Institute for Space Research, and part of the NASA Small Explorer program) in the 171 Å bandpass. The image represents plasma at roughly 1 MK.

3. The magnetically open corona can also lose energy through the acceleration of a solar wind. This is a very efficient energy loss mechanism that sets firm limitations on coronal electron and ion temperatures as described by Hansteen, Leer and co-workers [24, 25], but we will restrict our attention to the magnetically closed corona in the remainder of this discussion.

In short, when the plasma is dense, $n_{\rm e}n_{\rm H}$ is large and variations in the heat input can be dealt with by small changes in the plasma temperature which will remain on order 10^4 K or less (similar to the photospheric radiation temperature). Conduction on the other hand is very inefficient at these temperatures. However, the density drops exponentially with height, with a scale height of only some hundreds of kilometers for a 10^4 K plasma. The efficiency of radiative losses therefor drops very rapidly with height and *any* mechanical heat input will raise the temperature of the plasma. The temperature will continue to rise until thermal conduction can balance the energy input. Since thermal conduction varies with a high power of the temperature this does not happen until the plasma has reached 1 MK or so. Thus, we expect any and every heating mechanism to give coronal temperatures of

this order, and we must conclude that the amplitude of the observed coronal temperature is not a good guide to the mechanisms heating the corona.

4.1 The Transition Region

The argument used above necessarily implies that thermal conduction is the most important energy loss mechanism from the closed corona. This in turn means that the energy flux carried away from the site of coronal heating will mainly be carried by conduction and therefore roughly constant. As the temperature falls away from the heating site the plasma's ability to carry a heat flux decreases rapidly (as $T_e^{5/2}$) and the temperature gradient must become large to compensate. This process sets the structure of the transition region; the interface between the hot corona and the much cooler chromosphere is invariably sharp as shown schematically in figure 11.

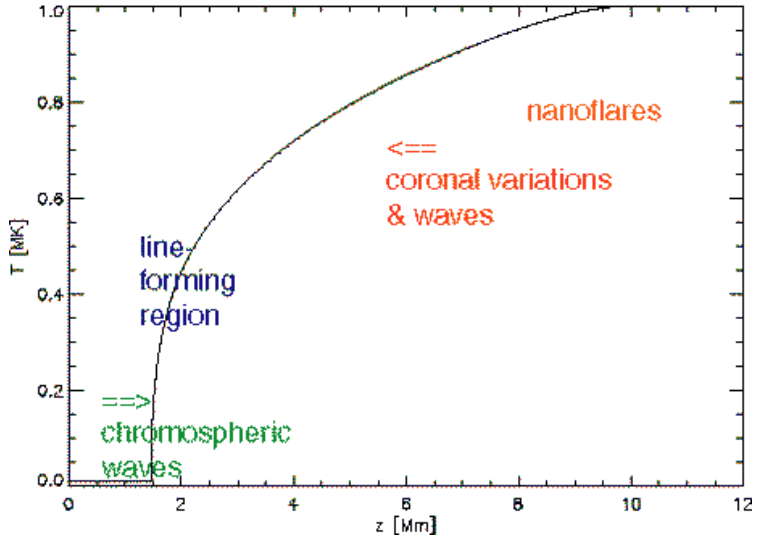

Fig. 11. Schematic structure of the transition region between chromosphere and corona: A more or less constant conductive flux from the corona ensures that the temperature gradient must steadily increase with decreasing temperatures until other terms (*e.g.* radiative losses) in the energy balance become significant. Optically thin spectral lines are formed over a relatively limited range in temperature and can therefore give good diagnostics of how the transition region responds to waves and other dynamic phenomena in the chromosphere below or the corona above.

With a very small spatial extent line formation in the transition region becomes particularly simple; the emission is optically thin and confined in space. Observations of transition region lines could therefore potentially be

both sensitive and understandable in terms of the processes heating both the chromosphere and corona.

Ions in the transition region will in general be in the ground state, excited occasionally by electron collisions followed immediately by a spontaneous de-excitation. Thus the intensity may be written

$$I_\nu = \frac{h\nu}{4\pi}\int_0^2 n_u A_{ul} ds = \frac{h\nu}{4\pi}\int_0^s n_l C_{lu} ds$$

where the integration is carried out along the line of sight, n_u and n_l are the upper and lower level populations of the emitting ion, A_{ul} is the Einstein coefficient, while C_{ul} is the collisional excitation rate. The other symbols retain their usual meanings. The lower level population may be rewritten

$$n_l = \frac{n_l}{n_i}\frac{n_i}{n_{\rm H}} n_{\rm H} = \frac{n_l}{n_i} A_i n_{\rm H}$$

where n_i is the total density of atoms of type i, n_l/n_i the degree of ionization, $n_{\rm H}$ the hydrogen number density, and A_i is the element abundance of atom i relative hydrogen. We may rewrite the collisional excitation rate as

$$C_{lu} = n_{\rm e} C_0 T_{\rm e}^{1/2} \exp\left(-\frac{h\nu}{kT_{\rm e}}\right) \Gamma_{lu}(T_{\rm e})$$

where C_0 is a constant and $\Gamma(T_{\rm e})$ is a slowly varying function of the electron temperature.

Combining the above allows us to rewrite the line intensity as

$$I_\nu = \frac{h\nu}{4\pi} A_i C_0 \int_0^s n_{\rm e} n_{\rm H} g(T_{\rm e}) ds \tag{3}$$

$$\propto E(T_{\rm e}) \equiv \int_{\Delta T{\rm e}} n_{\rm e} n_{\rm H} (ds/dT_{\rm e}) dT_{\rm e} \tag{4}$$

where we have defined the emission measure $E(T_{\rm e})$ by noting that the temperature dependent parts of the intensity may be collected into a rapidly varying function $g(T_{\rm e})$ that is sharply peaked around the region of maximum ion concentration n_l/n_i. The emission measure — as well as the differential emission measure, essentially the integrand of the emission measure, equation 4 — may be observationally determined from measured line intensities. Likewise given a corona heating model it is relatively straightforward to construct an expected emission measure. Comparisons of observed and predicted emission measures have met with little success; $E(T)$ has proven to be a difficult diagnostic for models to satisfy. In short, most if not all models predict much smaller line intensities for lines formed below 200 kK or so. To quote Grant Athay in a paper [26] written in 1982:

On the other hand, the total failure of all models for $T \lesssim 2.5 \times 10^5$ K is a clear indication that the models have either a grossly incorrect geometry or they are omitting or misrepresenting a fundamental energy transport process.

Another puzzling observation concerns the line shifts of lines formed in the transition region. Lines formed from the upper chromosphere/lower transition region (*e.g.* C II 133.4 nm) up to lines formed at temperatures of 500 kK are invariable red-shifted *on average* with the maximum red shift found for lines formed at roughly 100 kK (*e.g.* C IV 154.8 nm) of 10 km/s or greater. There is no reason to suppose that there is a net flow of material from the corona towards the chromosphere so some preferential weighting mechanism is implied. This effect is stronger in regions where the magnetic field is assumed strong, such as in the network and in active regions. And it is weaker or may be absent in the internetwork. Upwardly propagating sound waves, where plasma compression and the fluid velocity perturbation are in phase, would result in a net blue-shift. Does this imply that the red-shift is due to downwardly propagating waves formed, for example, as a result of nano-flare dissipation as suggested by Hansteen[27]? Or is some other mechanism insuring preferential emission of downward moving plasma active as claimed by *e.g.* Peter, Gudiksen & Nordlund [28]?

4.2 Forward Modelling

Simple and complex analytical models, semi-empirical modeling, and close analysis of the observations coupled with physical intuition have given researchers important insights into various aspects of the coronal heating question. However, it seems that this is not enough, the convection zone to corona system is of sufficient complexity to confound these methods as to the nature of coronal heating. Perhaps ab-initio numerical models can give insight into the problem?

It is only recently that computer power and algorithmic developments have allowed one to even consider taking on this daunting task. And still grave doubts remain on the validity of treating microscopic processes in the corona by the averaging methods inherent in the MHD approximation. The nano-flare scenario is based on photospheric shuffling and braiding resulting in the creation of discontinuities being formed in the coronal magnetic field. This implies that relatively large scale photospheric dynamics drives the coronal field to steadily smaller scales such that eventually the dissipation scale is reached and energy can be dissipated. Can we trust the results of calculations where this cascade is stopped by dissipation at scales many orders of magnitude larger than those presumably encountered in nature. And if it happens that we create a corona heating mechanism through our numerical modeling: How do we know it is the right one? We will come back to this and other connected issues in the last section of this chapter.

During the last few years the work of Gudiksen & Nordlund [29] has shown that it is possible to overcome the great numerical challenges outlined below to make initial attempts at modeling the photosphere to corona system. In their model a scaled down longitudinal magnetic field taken from an SOHO/MDI magnetogram of an active region is used to produce a potential

magnetic field in the computational domain that covers $50\times50\times30\,\mathrm{Mm}^3$. This magnetic field is subjected to a parameterization of horizontal photospheric flow based on observations and, at smaller scales, on numerical convection simulations as a driver at the lower boundary. After a period of some $10-15$ minutes solar time (and several months cpu time!) stresses in the simulated corona accumulate and become sufficient to maintain coronal temperatures. Synthetic TRACE images constructed from these models show a spectacular similarity to images such as figure 10. In addition other synthetic diagnostics *e.g.* of transition region lines show promising characteristics [28].

Numerical Challenges

There are several reasons that the attempt to construct forward models of the convection zone or photosphere to corona system has been so long in coming. We will mention only a few:

The size of the simulation. We mentioned in our description of potential field extrapolation that the magnetic field will tend to reach heights of approximately the same as the distance between the sources of the field. Thus if one wishes to model the corona to a height of, say, 10 Mm this requires a horizontal size close to the double, or 20 Mm in order to form closed field regions up to the upper boundary. On the other hand, resolving photospheric scale heights of 100 km or smaller and transition region scales of some few tens of kilometers will require minimum grid sizes of less than 50 km, preferably much smaller. (Numerical "tricks" can perhaps ease some of this difficulty, but will not help by much more than a factor two). Putting these requirements together means that it is difficult to get away with computational domains of much less than 150^3 — a non-trivial exercise even on todays systems.

Thermal conduction. The "Courant condition" for a diffusive operator such as that describing thermal conduction scales with the grid size Δz^2 instead of with Δz for the magnetohydrodynamic operator. This severely limits the time step Δt the code can be stably run at. One solution is to vary the magnitude of the coefficient of thermal conduction when needed. Another is to proceed by operator splitting, such that the operator advancing the variables in time is $L = L_{\mathrm{hydro}} + L_{\mathrm{conduction}}$. Thus the energy equation is solved by discretizing

$$\frac{\partial e}{\partial t} = \nabla \mathbf{F}_{\mathrm{c}} = -\nabla \kappa_{\parallel} \nabla_{\parallel} T$$

by the the Crank-Nicholson method and then solving the system by, for example the multigrid method[3].

[3] The general idea behind the multigrid method is to use Jacobi or Gauss - Seidel iterations, which are good at removing errors on small scales and bad at removing errors on large scales. Multigrid methods work by regridding the problem on successively coarser scales, thus converting large scales to small scales.

Radiative transport. Radiative losses from the photosphere and chromosphere are optically thick and will in principle require the solution of the transport equation. This can be done by the methods outlined in section 2.2 for the case of the photosphere which is close to LTE. Modeling the chromosphere may require that the scattering of photons is treated with greater care [11], or alternately that one may use methods assuming that chromospheric radiation can be tabulated as a function of local thermodynamic variables *a priori*.

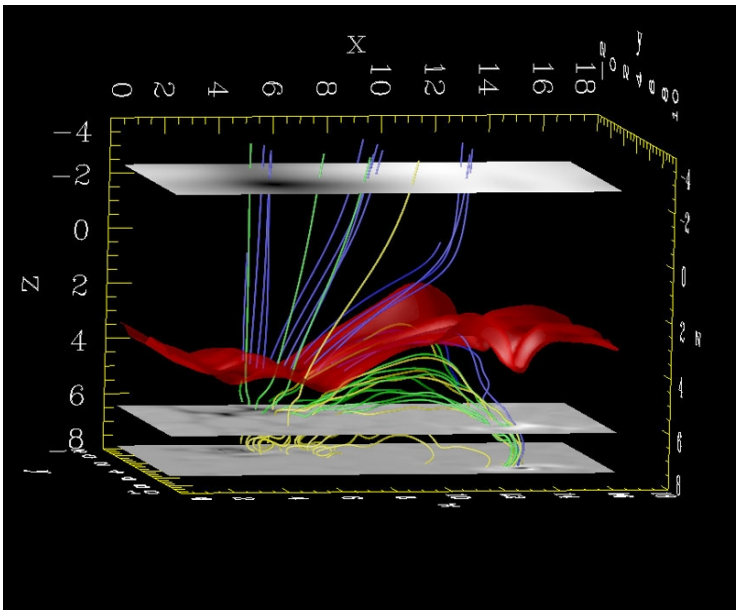

Fig. 12. The magnetic field structure as it has developed after some 20 minutes solar time evolution. Convection zone and photospheric motions have deformed the originally quite simple field. In the photosphere the field is quickly concentrated in inter-granular lanes. The black and white slabs show the vertical magnetic field B_z near the lower boundary and in the photosphere, as well as in the corona. The surface where where $T_g = 100$ kK is plotted in red. Some field lines are computed, starting from the lower convection zone (yellow), from the photosphere/lower chromosphere (green) and from the upper chromosphere/lower transition region (blue). Note also that the field lines below the photosphere seldom break the surface, rather they become quite tangled as a result of convective buffeting.

A concise introduction to multigrid methods may be found in Chapter 19 of "Numerical Recipes" [30]. The formulation used in the code described in this chapter is based on the method used by Malagoli, Dubey, Cattaneo as shown at `http://astro.uchicago.edu/Computing/On_ Line/cfd95/camelse.html`.

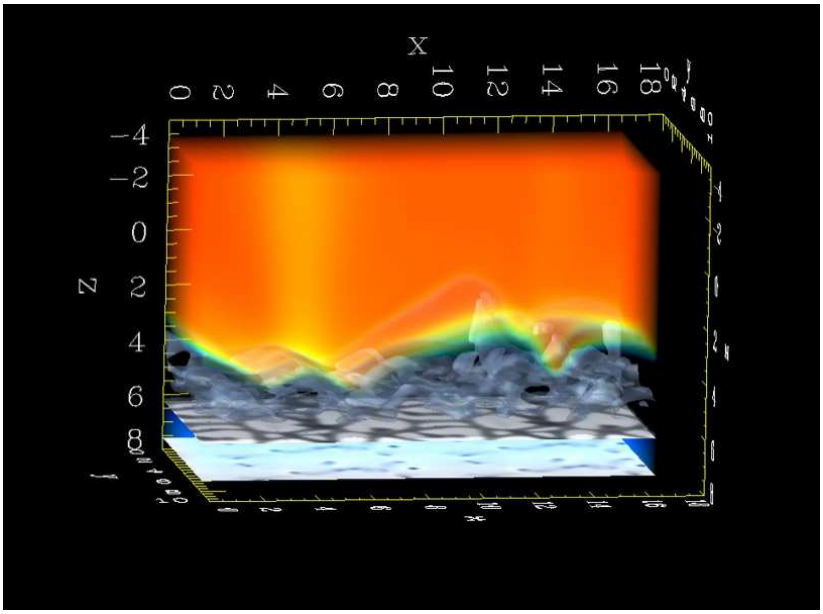

Fig. 13. The thermal structure of a 3d model as it has developed after some 20 minutes solar time evolution. Horizontal slices are shown near the lower boundary (where T_g is on order 15 000 K and in the photosphere. Isosurfaces of $T_g = 7000$ K are shown in the chromosphere, and coronal temperatures are shown in the colors blue (10^4 K) – red (6×10^5 K). The corona in this model is still cooling from its initial state where a uniform 8×10^5 K corona was imposed, but heating events are raising the temperature at certain coronal locations as the magnetic field is carried around by convective motions.

4.3 Convection Zone to Corona

With the proper tools in hand it is very tempting to attempt to model the entire solar atmosphere, from convection zone to corona. In figure 12 we show the result of such an experiment.

In a box of dimension 16×8×12 Mm^3 with well established convection we have inserted a potential magnetic field generated by setting up a source given by a positive and a negative pole with magnitude 1000 Gauss at the lower boundary. The models are convectively unstable due the radiative losses in the photosphere. The average temperature at the bottom boundary is maintained by setting the entropy of the fluid entering through the bottom boundary. The bottom boundary, based on characteristic extrapolation, is otherwise open, allowing fluid to enter and leave the computational domain as required. The magnetic field at the lower boundary is advected with the fluid. As the simulation progresses the field is advected with the fluid flow in

the convection zone and photosphere and individual field lines quickly attain quite complex paths through the model as shown in figure 12.

To prevent immediate coronal cooling the upper temperature boundary was initially set to a given temperature, 800 000 kK, and the models allowed to evolve from their potential state for 20 solar minutes. At this time the upper boundary was set so that the temperature gradient is zero; no conductive heat flux enters or leaves the computational domain. Aside from the temperature the other hydrodynamic variables and the magnetic field are set using extrapolated characteristics.

The temperature structure in the models is shown in figure 13. We find that the photosphere is found at a model depth of $z = 6$ Mm. The convection zone reaches down to the lower boundary some 2 Mm below, where the temperature is some 16 000 K. Above the photosphere the chromosphere stretches upwards to the transition region over a span varying between 1.5 Mm and 4 Mm above the photosphere. The corona fills the remaining 8 Mm or so of the computational domain, but regions of low temperatures are found at all depths up to $z = 0\ Mm$ and we expect that when the simulations have run longer there is no reason to believe that cool regions will not be found all the way up to the upper boundary.

Transition Region Diagnostics. There are several useful applications a model such as the one described here can be put to. Of these, perhaps the most interesting lies in studying the generation and dissipation of magnetic field stresses in the corona described in section 4.4. But there is also potential insight to be gained from studying the chromosphere and transition region is such models; 3d models of the magnetized chromosphere and transition region have been noticeably lacking. As an example let us consider the emission from the O VI 103.2 nm line formed in regions where the temperature is roughly 300 kK. In figure 14 we show the average line intensity and average line doppler shift as a function of time taken from a 2d model otherwise equivalent to the 3d model described above. The average magnetic field in this model has a fairly simple structure with a "loop" passing through the transition region with footpoints near $x = 4$ Mm and $x = 12$ Mm. The amplitude of the line emission is strong in regions where the magnetic field is nearly vertical, *i.e.* in the footpoints, and quite weak where the field is horizontal. The line shifts show that some signal of the chromospheric 3 minute oscillations reach the model transition region but at different times in regions of nearly vertical and nearly horizontal field. It is also interesting to note that the net-line shift does not vanish in the footpoints but rather displays an average red-shift of 10 km/s. These images are remarkably similar to images constructed from SOHO/SUMER observations of the same line and lead some confidence that this is a fruitful method for interpreting such observations.

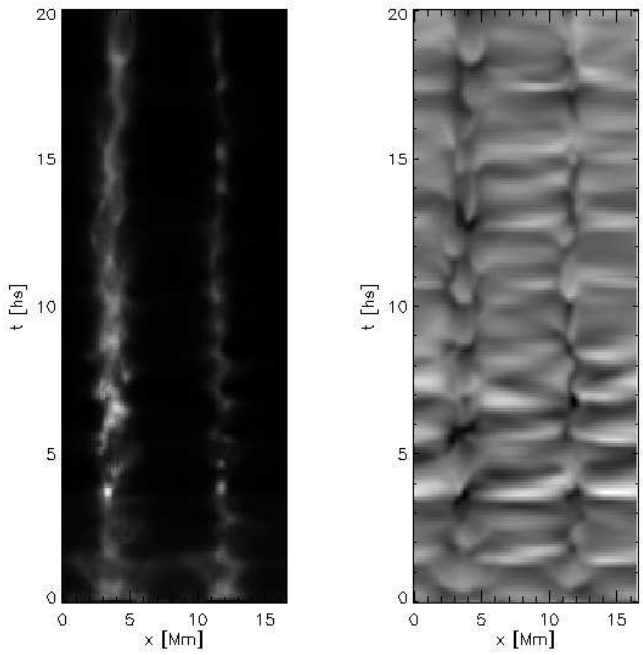

Fig. 14. Simulated observations of the O VI 103.2 nm line formed in regions where the temperature is roughly 300 kK. The left panel shows the total intensity in the line, the right panel shows the average Doppler shift. These simulated observations are based on a 2d MHD model spanning a region 16 Mm×10 Mm covering the convection to lower corona. The magnetic topology in this model is similar to that shown in figure 12: a "loop" with footpoints close to $x = 4$ Mm and $x = 12$ 12Mm. The periodic oscillations visible are mainly due upwardly propagating waves generated in the photosphere or below.

4.4 Modeling Nanoflares

As the stresses in the coronal field grow so does the energy density of the field. This energy must eventually be dissipated; at a rate commensurate with the rate at which energy flux is pumped in. On the Sun the magnetic diffusivity η is very small and gradients must become very large before dissipation occurs. In the models presented here we operate with an η many orders of magnitude larger than on the Sun and dissipation starts at much smaller magnetic field gradients. The dissipated energy is

$$Q_{\rm Joule} = \mathbf{E} \cdot \mathbf{J} \tag{5}$$

where $\mathbf{J} = \nabla \times \mathbf{B}$ is the current density and the resistive part of the electric field is given by

$$E_x^{\eta} = \left\{ \frac{1}{2}(\eta_y^{(1)} + \eta_z^{(1)}) + \frac{1}{2}(\eta_y^{(2)} + \eta_z^{(2)}) \right\} J_x \tag{6}$$

and similar for E_y and E_z. The diffusivities are given by

$$\eta_j^{(1)} = \frac{\Delta x_j}{\mathrm{Pr}_M}(v_1 c_f + v_2 |u_j|) \tag{7}$$

$$\eta_j^{(2)} = \frac{\Delta x_j^2}{\mathrm{Pr}_M} v_3 |\nabla_\perp \cdot \mathbf{u}|_- \tag{8}$$

where Pr_M is the magnetic Prandtl number, c_f is the fast mode speed, v_1, v_2 and v_3 are dimensionless numbers of order unity and the other symbols retain their usual meanings.

The working assumption in these models is then that the artificial magnetic diffusivity used here and the diffusivity found on the Sun differ by many orders of magnitude the total amount of energy actually dissipated in the chromosphere and corona should be similar [31, 32].

The following conclusions are among the results of this modeling effort so far:

- A non-heated non-magnetic corona will cool significantly within 1200 s to 1500 s. Even fairly strong hydrodynamic waves cannot maintain coronal temperatures.
- On the other hand it seems that coronae threaded by even fairly weak fields can be maintained at temperatures of greater than 700 000 K by the stresses developed through convective and photospheric motions.
- The average coronal temperature (and heating) rises with increasing magnetic field strength. The structure of the field may also have some importance, but perhaps mainly on the location (height) of the heating.
- Magnetic heating rates in the chromosphere are in part high and we expect to see signatures of magnetic chromospheric heating in simulated emission.

The way forward

It seems therefore that the modeling effort so far is very promising; a number of observational characteristics are reproduced in these models. Starting from an observed magnetic field and a parameterization of the solar velocity field in the photosphere as boundaries and drivers, one can reproduce images that look remarkably like those observed in the coronal TRACE bands. In addition, synthetic spectral lines calculated on the basis of these models show characteristics that are very similar to those seen in SUMER and CDS spectra as shown in figure 14 or by [28]. And this congruence between observations and model is achieved with what is in fact very few free parameters. Can we then conclude that the corona heating problem is solved?

Perhaps a word or two of caution is in order before we celebrate our successes. We do have a promising hypothesis, but the question remains:

Are the tests we are subjecting it to — *e.g.* the comparison of synthetic observations with actual observations actually capable of separating a correct description of the sun from an incorrect one? We have already demonstrated that we expect the solar corona to be heated to roughly 1 MK almost no matter what the mechanism for such heating. Conduction along field lines will naturally make loop like structures. This implies that reproducing TRACE-like "images" is perhaps not so difficult after all, and possible for a wide spectrum of coronal heating models. The transition region diagnostics are a more discerning test, but clearly it is still too early to say that the only possible coronal model has been identified. It will be very interesting to see how these forward coronal heating models stand up in the face of questions such as: How does the corona react to variations in the total field strength, or the total field topology, and what observable diagnostic signatures do these variations cause?

Another issue is the fact that the treatment of the microphysics of dissipation is demonstrably wrong in these models. As stated in the previous section, the argument can be made that this does not matter, that the only important factor entering the problem is the amount of Poynting flux entering the corona. The way this is dissipated, over what spatial and temporal scale, depends in part on the details of the microphysics, but the total amount of energy flux going into heating the corona remains the same and is independent of the exact physical process that thermalizes the Poynting flux. On the other hand, and persuasive as this argument may seem: It would be a large step forward to find diagnostics that could confirm even more firmly that the model described here is essentially correct.

One could also wonder about the role of emerging flux in coronal heating: How much new magnetic flux must be brought up from below in order to replenish the dissipation of field heating the corona? And what, if any, is the role of an eventual surface dynamo? The thermalization process is itself also of great interest. Is it highly episodic such as found in the work of [33]? Do the electric fields built up by the churning of the magnetic field cause particle acceleration to large energies as claimed by [34]? Is there a difference between the coronal heating mechanism and the process heating the network chromosphere? And what happens in open magnetic field regions where stresses built up by photospheric motions are free to propagate out into interplanetary space? There are certainly many open questions to be dealt with in the field of coronal heating, even if it should turn out that the basic scenario is correctly described by the current crop of forward models.

References

1. Stein, R. F. and Nordlund, A. Simulations of Solar Granulation. I. General Properties. ApJ, 499:914–+, May 1998.

2. Scharmer, G. B., Bjelksjö, K., Korhonen, T. K., Lindberg, B., and Petterson, B. The 1-meter Swedish solar telescope. In *Innovative Telescopes and Instrumentation for Solar Astrophysics. Edited by Stephen L. Keil, Sergey V. Avakyan . Proceedings of the SPIE, Volume 4853*, pages 341–350, 2003.
3. Berger, T., Rouppe van der Voort, L., Löfdahl, M., Carlsson, M., Fossum, A., Hansteen, V., Marthinussen, E., Title, A., and Scharmer, G. Solar magnetic elements at 0.1 arcsec resolution. A&A, 428:613–628, 2004. (Paper I).
4. Scharmer, G. B., Dettori, P. M., Löfdahl, M. G., and Shand, M. Adaptive optics system for the new Swedish solar telescope. In *Innovative Telescopes and Instrumentation for Solar Astrophysics. Edited by Stephen L. Keil, Sergey V. Avakyan . Proceedings of the SPIE, Volume 4853*, pages 370–380, 2003.
5. van Noort, M., Rouppe van der Voort, L., and Löfdahl, M. G. Solar Image Restoration By Use Of Multi-frame Blind De-convolution With Multiple Objects And Phase Diversity. Sol. Phys., 228:191–215, May 2005.
6. Muller, R. The dynamical behavior of facular points in the quiet photosphere. Sol. Phys., 85:113–121, May 1983.
7. Berger, T. E. and Title, A. M. On the Dynamics of Small-Scale Solar Magnetic Elements. ApJ, 463:365, May 1996.
8. Berger, T. E., Löfdahl, M. G., Shine, R. S., and Title, A. M. Measurements of Solar Magnetic Element Motion from High-Resolution Filtergrams. ApJ, 495:973, March 1998.
9. Nisenson, P., van Ballegooijen, A. A., de Wijn, A. G., and Sütterlin, P. Motions of Isolated G-Band Bright Points in the Solar Photosphere. ApJ, 587:458–463, 2003.
10. Nordlund, Å. Numerical simulations of the solar granulation. I - Basic equations and methods. A&A, 107:1–10, March 1982.
11. Skartlien, R. A Multigroup Method for Radiation with Scattering in Three-Dimensional Hydrodynamic Simulations. ApJ, 536:465–480, June 2000.
12. Carlsson, M., Stein, R. F., Nordlund, Å., and Scharmer, G. B. Observational Manifestations of Solar Magnetoconvection: Center-to-Limb Variation. ApJ, 610:L137–L140, August 2004.
13. Vernazza, J. E., Avrett, E. H., and Loeser, R. Structure of the solar chromosphere. III - Models of the EUV brightness components of the quiet-sun. ApJS, 45:635–725, April 1981.
14. Wikstøl, Ø., Hansteen, V. H., Carlsson, M., and Judge, P. G. Chromospheric and Transition Region Internetwork Oscillations: A Signature of Upward-propagating Waves. ApJ, 531:1150–1160, March 2000.
15. Sterling, A. C. and Hollweg, J. V. The rebound shock model for solar spicules - Dynamics at long times. ApJ, 327:950–963, April 1988.
16. Carlsson, M. and Stein, R. F. Does a nonmagnetic solar chromosphere exist? ApJ, 440:L29–L32, February 1995.
17. Fossum, A. and Carlsson, M. High-frequency acoustic waves are not sufficient to heat the solar chromosphere. Nature, 435:919–921, June 2005.
18. Seehafer, N. Determination of constant alpha force-free solar magnetic fields from magnetograph data. Sol. Phys., 58:215–223, July 1978.
19. Schrijver, C. J., DeRosa, M. L., Metcalf, T. R., Liu, Y., McTiernan, J., Regnier, S., Valori, G., Wheatland, M. S., and Wiegelmann, T. Nonlinear force-free modeling of coronal magnetic fields. i. a quantitative comparison of methods. Sol. Phys., 2006. In press.

20. Rosenthal, C. S., Bogdan, T. J., Carlsson, M., Dorch, S. B. F., Hansteen, V., McIntosh, S. W., McMurry, A., Nordlund, Å., and Stein, R. F. Waves in the Magnetized Solar Atmosphere. I. Basic Processes and Internetwork Oscillations. ApJ, 564:508–524, January 2002.
21. Bogdan, T. J., Carlsson, M., Hansteen, V. H., McMurry, A., Rosenthal, C. S., Johnson, M., Petty-Powell, S., Zita, E. J., Stein, R. F., McIntosh, S. W., and Nordlund, Å. Waves in the Magnetized Solar Atmosphere. II. Waves from Localized Sources in Magnetic Flux Concentrations. ApJ, 599:626–660, December 2003.
22. McIntosh, S. W., Bogdan, T. J., Cally, P. S., Carlsson, M., Hansteen, V. H., Judge, P. G., Lites, B. W., Peter, H., Rosenthal, C. S., and Tarbell, T. D. An Observational Manifestation of Magnetoatmospheric Waves in Internetwork Regions of the Chromosphere and Transition Region. ApJ, 548:L237–L241, February 2001.
23. McIntosh, S. W. and Judge, P. G. On the Nature of Magnetic Shadows in the Solar Chromosphere. ApJ, 561:420–426, November 2001.
24. Hansteen, V. H. and Leer, E. Coronal heating, densities, and temperatures and solar wind acceleration. J. Geophys. Res., 100:21577–21594, November 1995.
25. Hansteen, V. H., Leer, E., and Holzer, T. E. The Role of Helium in the Outer Solar Atmosphere. ApJ, 482:498–+, June 1997.
26. Athay, R. G. Responses of transition region models to magnetic field geometry and downflow velocities. ApJ, 263:982–986, December 1982.
27. Hansteen, V. A new interpretation of the redshift observed in optically thin transition region lines. ApJ, 402:741–755, January 1993.
28. Peter, H., Gudiksen, B. V., and Nordlund, Å. Coronal Heating through Braiding of Magnetic Field Lines. ApJ, 617:L85–L88, December 2004.
29. Gudiksen, B. V. and Nordlund, Å. Bulk Heating and Slender Magnetic Loops in the Solar Corona. ApJ, 572:L113–L116, June 2002.
30. Press, W. H., Flannery, B. P., Teukolsky, S. A., and Vetterling, W. T. *Numerical Recipes - Second Edition*. Cambridge University Press, Cambridge, 1988.
31. Galsgaard, K. and Nordlund, Å. Heating and activity of the solar corona 1. Boundary shearing of an initially homogeneous magnetic field. J. Geophys. Res., 101:13445–13460, June 1996.
32. Hendrix, D. L., van Hoven, G., Mikic, Z., and Schnack, D. D. The Viability of Ohmic Dissipation as a Coronal Heating Source. ApJ, 470:1192–+, October 1996.
33. Einaudi, G. and Velli, M. The distribution of flares, statistics of magnetohydrodynamic turbulence and coronal heating. *Physics of Plasmas*, 6:4146–4153, November 1999.
34. Turkmani, R., Vlahos, L., Galsgaard, K., Cargill, P. J., and Isliker, H. Particle Acceleration in Stressed Coronal Magnetic Fields. ApJ, 620:L59–L62, February 2005.